International Journal for Modern Trends in Science and Technology
Volume 12, Issue 04, pages 1357-1366.
ISSN: 2455-3778 online
Available online at: http://www.ijmtst.com/vol12issue04.html
DOI: https://doi.org/10.5281/zenodo.18733837

A High-Efficiency EV Charging Framework Using Hybrid Renewable Energy and High-Gain Interleaved Converter with ANN-Optimized MPPT

R.V.V. Satyanarayana

Department of Electrical and Electronics Engineering, Sri Sarathi Institute of Engineering Technology, Nuzvid, AP, India.

To Cite this Article
R.V.V. Satyanarayana (2026). A High-Efficiency EV Charging Framework Using Hybrid Renewable Energy and High-Gain Interleaved Converter with ANN-Optimized MPPT. International Journal for Modern Trends in Science and Technology, 12(04), 1357-1366. https://doi.org/10.5281/zenodo.18733837

Article Info
Received: 17 March 2026; Revised: 12 April 2026; Accepted: 16 April 2026.

KEYWORDS

PV system,
HGIB converter,
FSO based ANN-MPPT controller,
DFIG-WECS and Battery.

ABSTRACT

This research presents a hybrid renewable energy-based Electric Vehicle (EV) charging system. A photovoltaic (PV) array is interfaced with a High-Gain Interleaved Boost (HGIB) converter to step up the PV voltage to the required DC bus level. A Flying Squirrel Optimized Artificial Neural Network (FSO-ANN) is employed for Maximum Power Point Tracking (MPPT), ensuring accurate power extraction under varying environmental conditions. Concurrently, a Doubly Fed Induction Generator (DFIG) provides supplementary power to the DC bus through a PWM rectifier. Energy exchange between the DC bus and EV battery is managed by a bidirectional buck-boost converter, supporting both charging and discharging operations. MATLAB/Simulink simulation results demonstrate that the proposed system improves grid stability, achieving an efficiency of 95.23%. This approach establishes a robust framework for future EV charging infrastructure, promoting the adoption of environmentally friendly electric vehicles.

1. INTRODUCTION

Electric Vehicles (EVs) offer numerous socioeconomic and environmental benefits, motivating governments worldwide to transition traditional transportation systems toward greener alternatives. Although EVs do not directly consume fossil fuels, their reliance on electricity from fossil fuel-based grids indirectly contributes to fossil fuel usage [1]. To address this issue, researchers are exploring cost-effective and environmentally friendly renewable energy sources to bridge the gap between electricity supply and demand. Rising environmental and economic constraints have accelerated the adoption of renewable energy systems (RES) such as solar, wind, and fuel cells, promoting distributed generation and energy conservation [2].

A widely studied approach is the integration of renewable energy, particularly photovoltaic (PV) and wind energy, to meet the growing electricity demand for EV charging [3]. While solar panels generate power primarily during daylight hours, wind turbines can produce electricity continuously, providing a reliable complement to solar energy [4]. Combining multiple renewable sources ensures a more stable and dependable energy supply. Additionally, surplus energy generated during peak production periods can be stored in battery systems, guaranteeing a continuous power source for EV charging even when generation is low [5]. However, the inherent variability and intermittency of renewable energy pose challenges, potentially reducing system reliability and security when integrated for EV charging applications [6, 7].

The Double Boost Converter is utilized in grid, electric vehicle and renewable energy applications. The primary goal this converter is to increase the output voltage by four times while using the lowest components. Additionally, due to higher conduction and switching losses, the converter often experiences decreased efficiency at high load conditions [8]. In terms of voltage stress and gain, a high gain quadratic boost converter [9] has demonstrated promising superiority. However, because of the larger load currents, efficiency decreases as duty cycle increases.

A Z-source converter [10] maintains low voltage strains on the switch and diode while achieving a larger voltage gain at the similar duty ratio. However, the efficiency is comparatively low because of the higher current root mean square value and larger current ripple. To generate a maximum voltage suitable for DC micro grid and EV charging systems, the modified SEPIC converter [11] combines a coupled inductor with a voltage boosting section. Nevertheless, it incorporates additional components, including many switches and inductors, which increases the component failure.

Then, the interleaved boost converter [12] has reduced current ripple and minimized current pressure. Nevertheless, it has high component stress due to its increased components. The high step-up converter [13] has the ability to boost voltage levels, allowing compatibility with high-voltage devices and grid systems. Nevertheless, it affected from reduced efficacy because of switching losses and electromagnetic interference, especially under heavy load conditions. Therefore, the High-Gain Interleaved Boost converter is developed to improve the voltage. Subsequently, the PV array voltage is modified to match the highest output power.

The conventional MPPT algorithm comprises Perturb and Observe [14], Incremental Conductance [15] and Hill Climbing [16] approaches. However, that methods has unpredictability and poor tracking performance during fluctuating weather and cause inefficiencies due to constant perturbations but its performance is improved by the optimization algorithm [17] are Ant colony optimization [18], Genetic algorithm [19], Salp Swarm [20], Cat swarm [21] and cuckoo search [22]. However, that approaches has get stuck in local optima, converge prematurely to suboptimal solutions, suffer from slow convergence, difficult parameter tuning and low performance. Thus, the Flying Squirrel Optimized ANN-MPPT controller is exploited to track the highest power from PV system. The main objectives are,

- The HGIB Converter is developed to improve the voltage level of PV system that is appropriate for interaction with grid and batteries.
- The ANN-MPPT controller is employed for tracking the maximum power from PV system and its parameters are fine-tuned by FSO algorithm.
- The DFIG-WECS is developed for providing the energy supply to charge the electric vehicles.
- The battery system is exploited for storing the excess energy from HRES system and bidirectional buck-boost converter facilitate both discharging and charging functions of the battery.

II. PROPOSED METHODOLOGY

The block diagram for HRES based EV charging station is represented in Figure 1. In the beginning, the low voltage of PV system is improved with the aid of HGIB converter. Then, the highest power of PV system is tracked by exploiting an ANN-MPPT controller and its parameters are fine-tuned by a FSO algorithm. Subsequently, the PWM generator produce PWM pulses for managing the switching operation of the developed converter. Meanwhile, the AC output of DFIG-WECS is transformed into DC power with the assistance of PWM rectifier. A PI controller sustains the reference voltage by comparing it with actual voltage from the DFIG and

resulting signal is exploited by a PWM generator to regulate the rectifier operation.

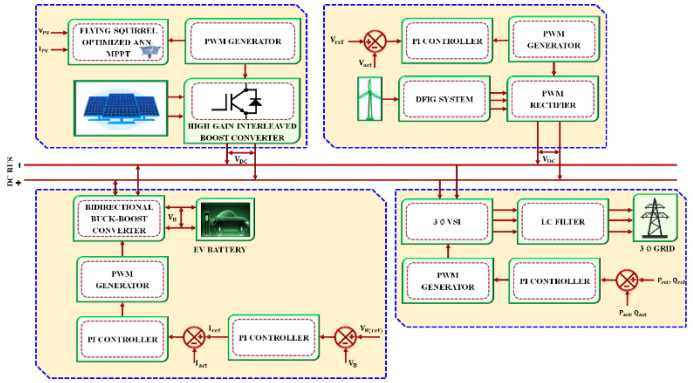

Figure 1 Block diagram of PV-DFIG system

Furthermore, the battery is utilized to store the excess energy from HRES and its discharging and charging operation is carried out by bidirectional buck-boost converter. Here, the PI controller is used to manage the function of a battery voltage and current with respect to their reference values to sustain the proper energy flow. Thus, the DC power is delivered to the 3ϕ VSI, which transforms the DC-AC power and LC filter assures the reduced harmonics power is supplied to the 3ϕ grid. It provides a robust solution for grid and EV charging stations.

A) PV SYSTEM

Solar modules are the collection of PV cells and the modules in parallel and series manner creates an array. It has the diode (D), current source (I_{Ph}), shunt resistor (R_{Sh}) and series resistor (R_{Se}). Figure 2 reveals the circuit of PV system.

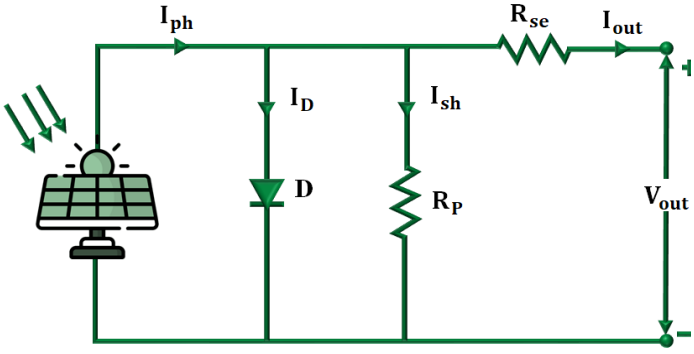

Figure 2 Circuit of PV system

The output current of a PV system is,

$$I_{Out} = I_{Ph} - I_D - I_{Sh} \quad (1)$$

$$I_{Out} = I_{Ph} - I_S\left[e^{\frac{V_{Out}+I_{Out}R_{Se}}{nVt}-1}\right] - \frac{V_{Out}+I_{Out}R_{Se}}{R_{Sh}} \quad (2)$$

An output power from the PV system is relational to the irradiance level that is exposed to variation at every time and is improved by a developed converter.

B) HGIB CONVERTER

A HGIB converter enhances the voltage to a maximum level, as seen in Figure 3. The switching waveform of this converter is displayed in Figure 4.

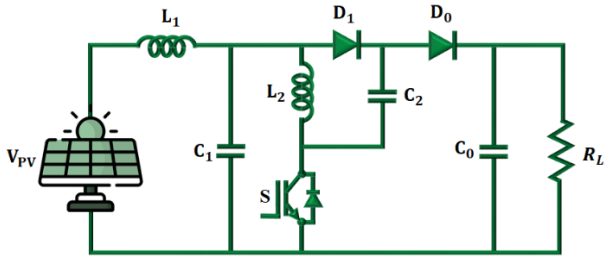

Figure 3 Structure of HGIB converter

Mode 1

When S is active, V_{PV} is supplies the power to charge L_1 andL_2. Here, D_1 is conducting that enables the current flow via L_2 and C_2, leads to charging of C_2. Since, D_0 is inactive and C_0 powers the load, as revealed in Figure 5(a).

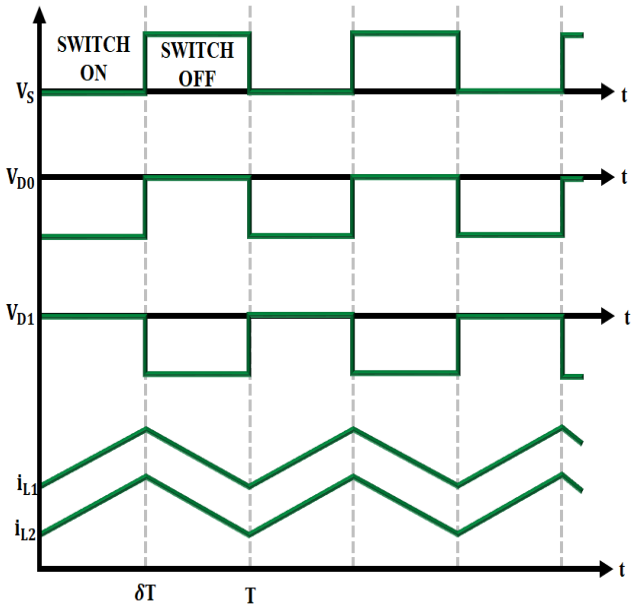

Figure 4 Switching waveform of HGIB converter

Mode 2

This stage is initiated when S is inactive, L_1 and L_2discharge their stowed energy that is transformed towards output side. D_0 becomes forward biased, enabling the current to flow and deliver energy from L_2 and C_2 toC_0 and load, as presented in Figure 5(b).

By applying KVL in stage 1,

$$V_{L1} = V_{PV} \quad (3)$$

$$V_{L2} = V_{PV} - V_{C1} \quad (4)$$

$$V_{C2} = V_{C1} \quad (5)$$

$$V_0 = V_{C0} \quad (6)$$

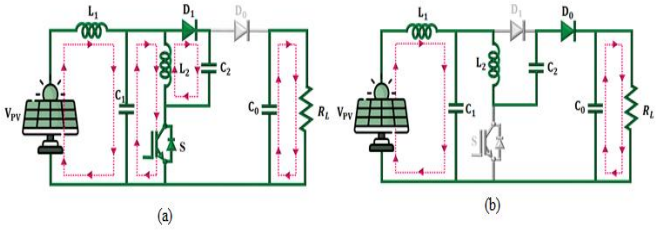

Figure 5 Modes of HGIB converter (a) Stage 1 (b) Stage 2

By applying KVL in stage 2,

$$V_{L1} = V_{PV} - V_{C1} \quad (7)$$

$$V_{L2} = V_{C1} - V_{C2} \quad (8)$$

$$V_0 = V_{C1} + V_{C2} \quad (9)$$

$$V_{C1} = V_{C2} \quad (10)$$

$$V_0 = 2V_{C1} \quad (11)$$

By applying Volt-second balance law,

$$\delta V_{PV} + (1-\delta)(V_{PV} - V_{C1}) = 0 \quad (12)$$

$$V_{C1} = \frac{V_{PV}}{1-\delta} \quad (13)$$

$$V_0 = 2V_{C1} - \delta V_{C1} \quad (14)$$

$$\frac{V_0}{V_{PV}} = \frac{2-\delta}{(1-\delta)^2} \quad (15)$$

Thus, the converter enhances the voltage of PV system and its performance is improved by the ANN-MPPT controller with FSO algorithm is utilized that is discussed in the upcoming section.

C) FLYING SQUIRREL OPTIMIZED ANN-MPPT CONTROLLER

An ANN-MPPT algorithm is utilized to dynamically modify the PV 's operating point in order to maximize power extraction under a variable conditions. The weights in each layer of the neural network are changed during training until the intended results are obtained. The MSE is,

$$F = \frac{1}{N}\sum_{i=1}^{N}[t_i - a_i]^2 \quad (16)$$

Where, the present output is denoted by a_i and target is t_i.

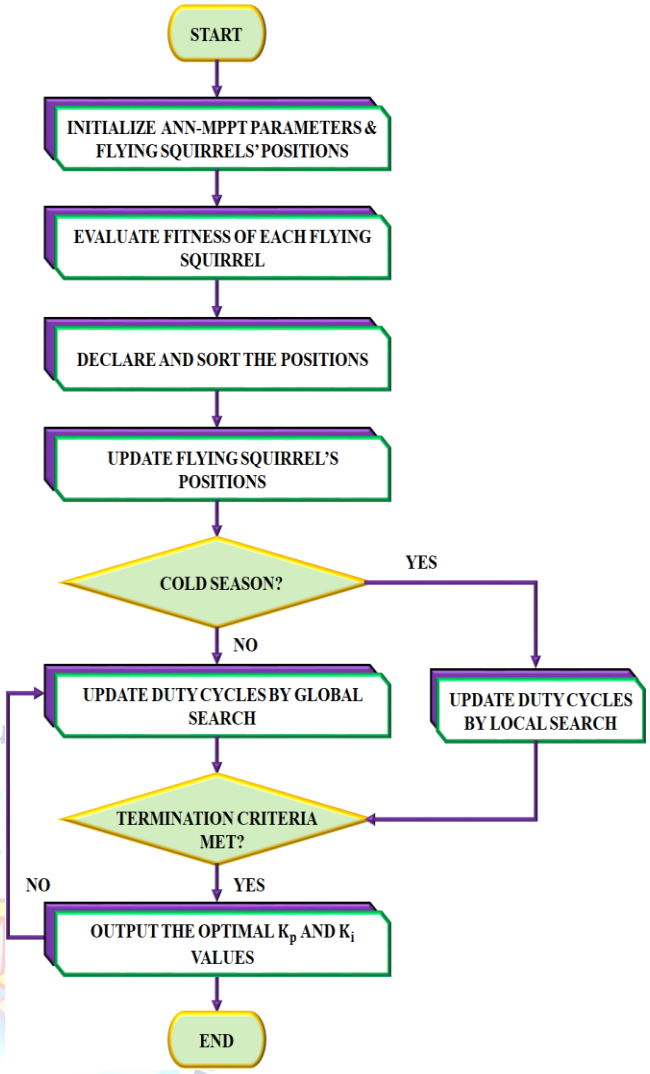

Figure 6 Flowchart of FSO based ANN-MPPT controller

In the ANN-MPPT controller, the parameters that affect its performance are weights, biases and predicted duty ratio of the developed converter. In the initialization phase, each squirrel is assigned a unique position according to the duty ratio,

$$d_i = d_{mn} + \frac{(i-1)[d_{mx}-d_{mn}]}{N_{fs}}; i = 1,2,\cdots,N_{fs} \quad (17)$$

Where, the maximum and minimum values of converter duty ratio are indicated by d_{mx} and d_{mn}. The constraint limits on duty ratio are,

$$0 < d_i < 0.5 \quad (18)$$

In the fitness evaluation phase, each squirrel's current position corresponds to a particular duty ratio that is applied to the converter. The fitness function is,

$$f(d) = maxP_{PV}(d) \quad (19)$$

In the declaration and sorting phase, once the fitness values for all flying squirrels are evaluated, the duty ratio that generates the maximum output power is declared as the position of hickory tree, which indicates the global best solution and becomes the main target of

all other flying squirrel to glide toward in future iterations. The next best duty ratio that gives the second highest output power is classified as the acorn tree that served as a local best, which aids to promote diversity in exploration. The remaining flying squirrels are located on normal tree, which indicate suboptimal regions of the search space. In the position update phase, the duty cycle associated with each flying squirrel is updated based on seasonal monitoring. The seasonal monitoring condition is introduced to prevent the algorithm from getting trapped in local maximum power points during the optimization of ANN-MPPT controller. It mimics the real world seasonal adaptation and assures a balance among exploration and exploitation.

$$S_K^C = \left| d_{at}^k - d_{ht} \right| \quad (20)$$

The minimum seasonal threshold is,

$$S_{min} = \frac{10e^{-6}}{(365)^k/(k_m/2.5)} \quad (21)$$

Where, the maximum number of iterations are k_m and current iteration number is k. If $S_K^C < S_{min}$, duty ratios of flying squirrels on normal trees are updated using Levy flight based exploration that introduces long jumps to escape local optima.

$$d_{nt}^{k+1} = d_{nt}^k + s \quad (22)$$

Where, s is the step length derived from Levy distribution that is given by,

$$s \approx k\left(\frac{u}{|v|^{\frac{1}{\beta}}}\right)(d_{ht} - d_{nt}) \quad (23)$$

The random variables are,

$$u \approx N(0, \sigma_u^2) \quad (24)$$

$$u \approx N(0, \sigma_v^2) \quad (25)$$

The standard deviation are computed by,

$$\sigma_u = \left(\frac{\Gamma(1+\beta)sin(\pi\beta/2)}{\Gamma\left(\frac{(1+\beta)}{2}\right)\beta(2)^{\left(\frac{\beta-1}{2}\right)}}\right)^{\frac{1}{\beta}} \quad (26)$$

$$\sigma_v = 1 \quad (27)$$

$$\Gamma(n) = (n-1)! \quad (28)$$

It assures the random yet directed exploration around the d_{ht} pushing the flying squirrels toward the most promising regions of search space. In the routine update phase, the positional update strategy is applied to refine the duty ratio value associated with each squirrel based on its tree classification. The squirrel in the acorn tree performs a directed glide toward the hickory tree by,

$$d_{at}^{k+1} = d_{at}^k + g_d G_c\left(d_{ht}^k - d_{at}^k\right) \quad (29)$$

$$d_{nt}^{k+1} = d_{nt}^k + g_d G_c\left(d_{ht}^k - d_{nt}^k\right) \quad (30)$$

$$d_{nt}^{k+1} = d_{nt}^k + g_d G_c(d_{at}^k - d_{nt}^k) \quad (31)$$

Where, the gliding constant is denoted as G_c and gliding distance is g_d. This hierarchical movement assures both exploitation of the best known solutions and diversification via alternate gliding paths. The gliding distance is,

$$g_d = \frac{h_g}{s_f tan\Phi} \quad (32)$$

$$tan\Phi = \frac{F_D}{F_L} \quad (33)$$

Where, the lift force and drag force is F_L and F_D, height loss is h_g and scaling factor is s_f.

$$F_D = \frac{1}{2}\rho V^2 S C_D \quad (34)$$

$$F_L = \frac{1}{2}\rho V^2 S C_L \quad (35)$$

In the convergence determination phase, the process is terminated based on 2 conditions. First, if the variation in the all flying squirrel's position becomes lesser than a predefined threshold. Second, the algorithm also terminated if the highest iterations are got. In the re-initialization phase, a variation in solar power triggers a restart of optimization process.

$$\frac{P_{PV}^{K+1} - P_{PV}^K}{P_{PV}^{K+1}} \geq \Delta P(\%) \quad (36)$$

It enables to adaptively search for a new MPP assuring the ANN-MPPT controller remains efficient. Here, the MPPT controller not only optimizes the duty ratio but also maintains high tracking accuracy over a wide range of solar input variations. The efficacy of the system is improved by another RES (DFIG) is utilized in this research.

D) DFIG-WECS

The purpose of DFIG is to produce electrical energy, as it transforms the energy from the wind power into electrical energy. In the $d-q$ frame, the electrical equation is,

$$V_{dr} = R_r I_{dr} - (w_s - w_r)\Psi_{qr} + \frac{d\Psi_{dr}}{dt} \quad (37)$$

$$V_{qr} = R_r I_{qr} + (w_s - w_r)\Psi_{dr} + \frac{d\Psi_{qr}}{dt} \quad (38)$$

$$V_{qs} = R_s I_{qs} + w_s \Psi_{ds} + \frac{d\Psi_{qs}}{dt} \quad (39)$$

$$V_{ds} = R_s I_{ds} - w_s \Psi_{qs} + \frac{d\Psi_{sd}}{dt} \quad (40)$$

Where, the rotor and stator resistance are R_r and R_s, angular frequencies of stator and rotor are w_s and w_r.

$$\Psi_{dr} = L_r I_{dr} + M I_{ds} \quad (41)$$

$$\Psi_{qr} = M I_{qs} + L_r I_{qr} \quad (42)$$

$$\Psi_{qs} = M I_{qr} + L_s I_{qs} \quad (43)$$

$$\Psi_{ds} = L_s I_{ds} + M I_{dr} \quad (44)$$

The rotor and stator inductances are denoted by L_r and L_s and magnetizing inductance is M.

$$Q_s = 1.5 \times \left(-I_{qs} \times V_{ds} + V_{qs} \times I_{qs}\right) \quad (45)$$

$$P_s = 1.5 \times \left(V_{qs} \times I_{qs} + I_{ds} \times V_{ds}\right) \quad (46)$$

$$V_{qs} = V_s = w_s.\Psi_s \quad (47)$$

$$V_{ds} = \frac{d\Psi_{ds}}{dt} = 0 \quad (48)$$

$$Q_s = -1.5\left(\frac{\omega_s \Psi_s M}{L_s} I_{dr} - \frac{\omega_s \psi_s^2}{L_s}\right) \quad (49)$$

$$P_s = -1.5\frac{V_s M}{L_s} I_{qr} \quad (50)$$

The expressions for rotor voltage are,

$$V_{qr} = R_{dr} I_{qr} + \sigma . L_r \frac{dI_{qr}}{dt} + \sigma g w_r L_r I_{dr} + w_r g \frac{M.\Psi_s}{L_s} \quad (51)$$

$$V_{dr} = R_{dr} I_{dr} - \sigma g w_r L_r I_{qr} + \sigma . L_r \frac{dI_{dr}}{dt} \quad (52)$$

$$\sigma = 1 - \frac{M^2}{L_s L_r} \quad (53)$$

Furthermore, the batery system is used for storing the excess energy from HRES.

E) BATTERY

When the RES are unavailable or the system is under peak load, the battery bank that is accessible in EVCS offers the energy. During the charging process, the surplus energy produced is kept in the battery. The charging process of the battery is,

$$E_{Bat}(t) = (1-\sigma) \times E_{Bat}(t-1) + (E_G(t) - E_L(t)/\eta_{conv}) \times \eta_{CC} \times \eta_{rbat}$$

Where, the converter's efficiency is η_{conv}, battery's round trip efficiency is η_{rbat}, charge controller's efficiency is η_{CC}, generated energy is E_G, electrical load demand is E_L and battery's energy levels are $E_{Bat}(t)$ and $E_{Bat}(t-1)$.

$$E_G(t) = [E_{DC}(t) + E_{AC}(t)] \times \eta_{conv} \quad (54)$$

The generated DC energy is,

$$E_{DC}(t) = E_{Pv}(t) + E_{WT}(t) \quad (55)$$

Produced AC energy is,

$$E_{AC}(t) = E_{BMG}(t) \quad (56)$$

The electrical energy produced by RES during the discharge process is less than the load that the battery bank and is given as,

$$E_{Bat}(t) = (1-\sigma) \times E_{Bat}(t-1) + (E_G(t) - E_L(t)/\eta_{conv}) - E_G(t)/\eta_{rbat} \quad (57)$$

III. RESULT AND DISCUSSIONS

This section analyses the outcomes of HRES based EV charging station in MATLAB/Simulink tool and analysis of traditional approaches are also provided. The Specification of parameters is indicated in Table 1.

Table 1 Specification of parameters

Parameters	Specification
PV system	
Total Power	15KW
Current (Short circuit)	8.95 A
Maximum Peak Voltage	29.95 V
Panel's peak power	250 W
Voltage (Open circuit)	37.25V
Maximum Peak Current	8.35 A
Series connected cells	6
Number of cells in shunt connection, N_P	10
DFIG	
Power	10 kW
Number of Turbine	4
Voltage	600 V
High-Gain Interleaved Boost converter	
C_1, C_2	22 μF
C_0	2200 μF
L_1, L_2	4.7 mH
Switching frequency f	10kHz

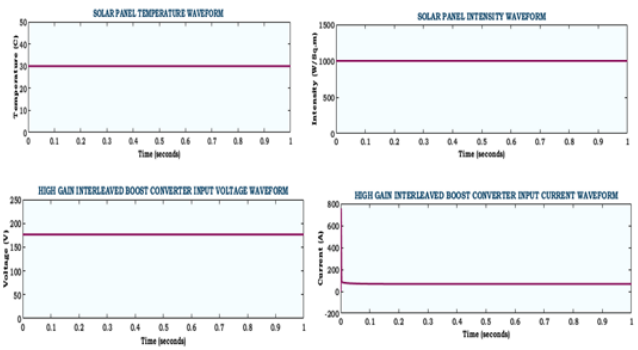

Figure 7 Characteristics of PV system

Figure 7 displays the characteristics of PV system in constant condition, in which the temperature and intensity are stabilized at a steady value of 30°C and 1000$(W/Sq.m)$. Then, the voltage on input side is sustained at 175 V while the input current is sustained at a static value of 80 A with no variations. Then, an input voltage is boosted with the aid of HGIB converter.

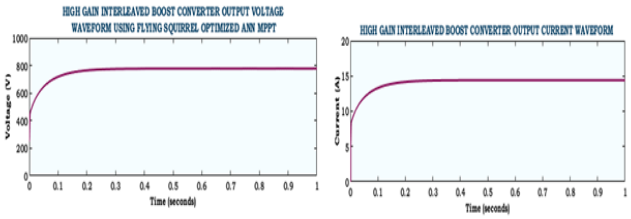

Figure 8 Output waveform of converter

An output waveform of developed converter is represented in Figure 8. The output voltage is initially raised and settled at 780V with the aid of FSO based ANN-MPPT controller. Consequently, an output current is sustained at 14 A with no oscillations.

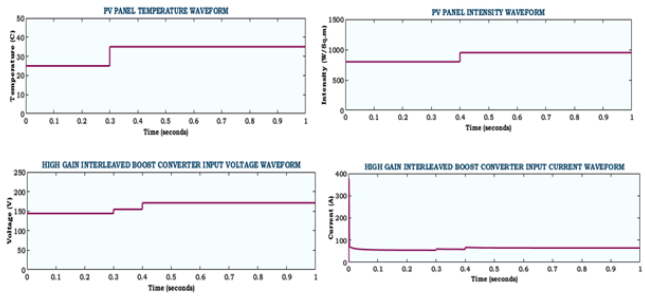

Figure 9 Behaviour of PV system

Figure 9 depicts the behaviour of PV system in varying condition. The values of temperature and intensity are gradually increased and stabilized at 35℃ and 900$(W/Sq.m)$. Here, the input voltage is varied in the beginning and sustained at 175 V and an input current is maintained at 60 A with no oscillations.

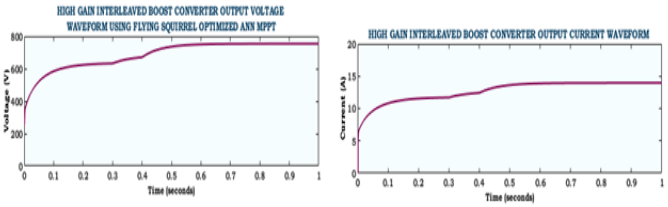

Figure 10 Output waveform of converter

An Output waveform of converter is revealed in Figure 10. The output voltage is randomly varied and sustained at 780V meanwhile the output current is slowly raised and maintained at 14A in the entire system.

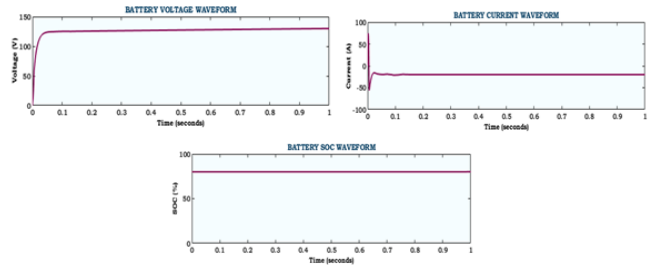

Figure 11 Waveform of battery

The waveform of battery is presented in Figure 11. The voltage of battery is gradually raised and maintained at 130 V and current of battery is settled at a reduced value while the SOC of battery is stabilized at 80 %.

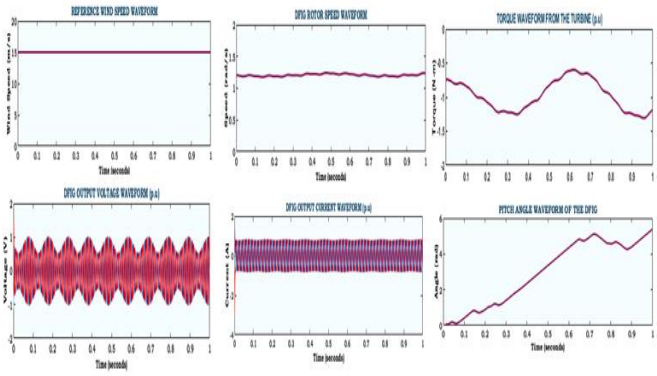

Figure 12 Waveform of WECS

The waveform of WECS is depicted in Figure 12. The wind speed is sustained at 15 (m/s) throughout the system while the speed of rotor is maintained at 1.25(rad/s) with more oscillations. Then, the torque is randomly varied and settled at a reduced value. Subsequently, an output voltage is steadied at a unity value whereas the output current is kept at 1A and pitch angle is randomly varied in the beginning and stabilized at 5.6 rad.

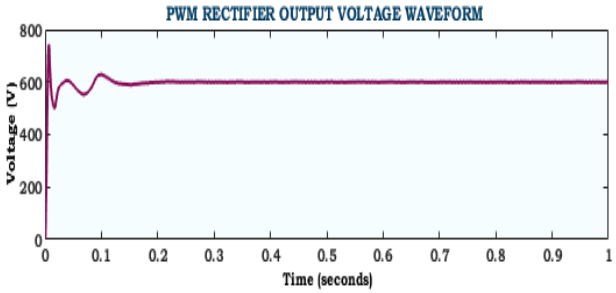

Figure 13 Waveform of PWM rectifier

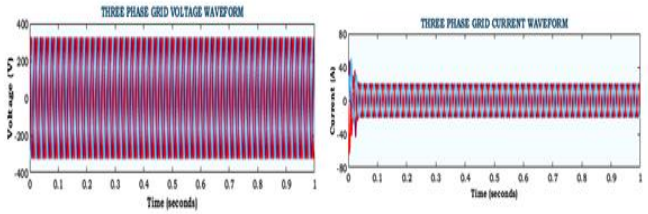

Figure 14 Waveform of grid

Figure 13 represents the waveform of PWM rectifier. The output voltage of PWM rectifier is randomly varied in the beginning and settled at 600 V with little fluctuations. The waveform of grid is depicted in Figure 14. Then, the grid's voltage is maintained a steady value of 320 V while the current of grid is varied randomly and stabilized at 20 A without fluctuations.

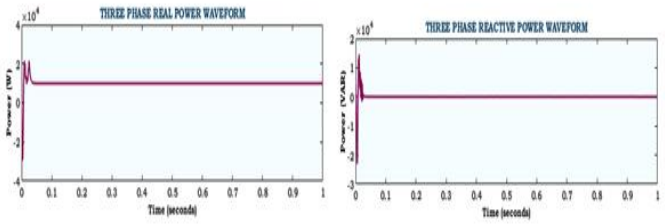

Figure 15 Waveform of power

The waveform of power is revealed in Figure 15. The real power is oscillated in the beginning and sustained at 1000 W while the reactive power is stabilized at a lesser value, representing the efficacy of the system is enhanced.

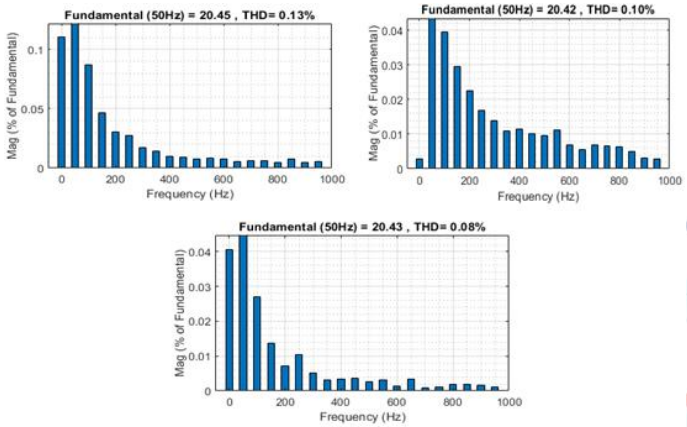

Figure 16 Waveform of THD

The waveform of THD is revealed in Figure 16. The B phase attains the lowermost THD of 0.08% compared to R and Y phase (0.13% and 0.10 %), indicating the power quality is enhanced with better performance.

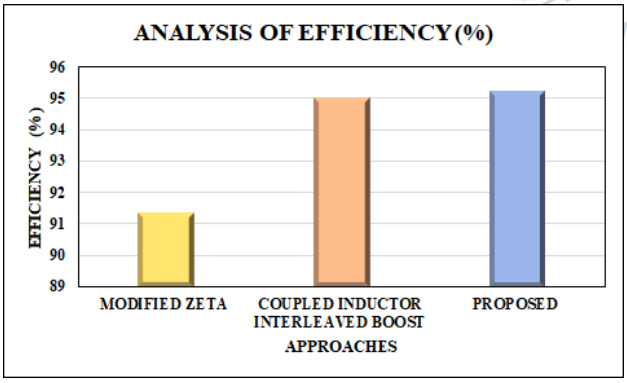

Figure 17 Comparison of efficiency

The comparison of efficiency for modified Zeta [23], Interleaved boost [24] and developed converter is shown in Figure 17. The modified Zeta converter has lowest value of 91.33% while the Interleaved boost converter attains 95% that is worse than HGIB converter with 95.23%, improves the overall reliability of the system.

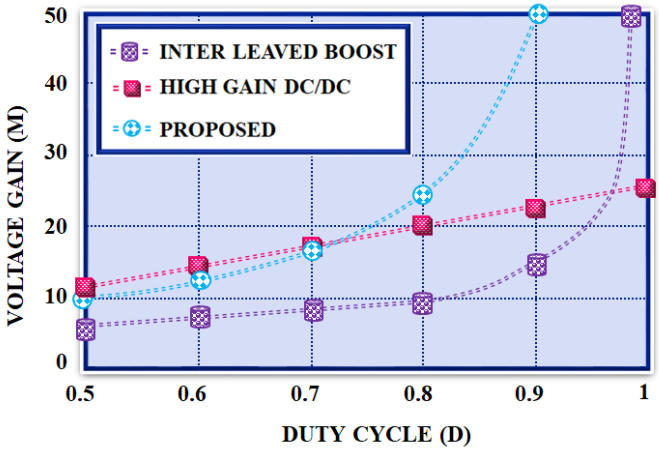

Figure 18 Comparison of voltage gain

Figure 18 displays the analysis of voltage gain with Interleaved boost [25], high gain [26] and HGIB converter that has demonstrates superior performance in attaining voltage gain while other converters has lesser voltage gain, indicates its strong capability for high voltage conversion.

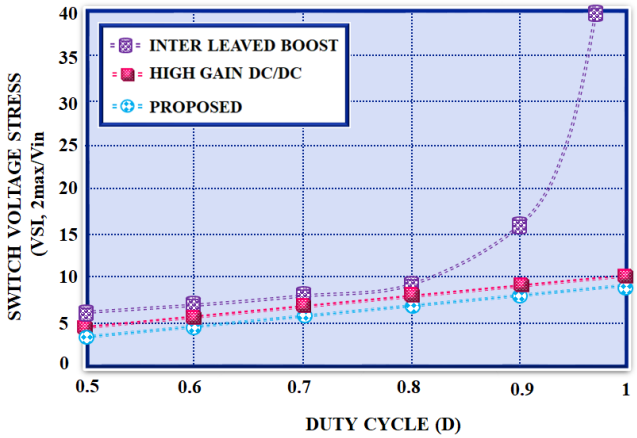

Figure 19 Comparison of voltage stress

The comparison of voltage stress for Interleaved boost [25], high gain [26] and developed converter. The Interleaved Boost shows a significant increase in voltage stress, indicating high component stress. The High gain converter maintains moderate voltage stress. The proposed approach consistently shows the lowest voltage stress across all duty cycles, emphasizing its superior ability in diminishing switch stress and improving reliability.

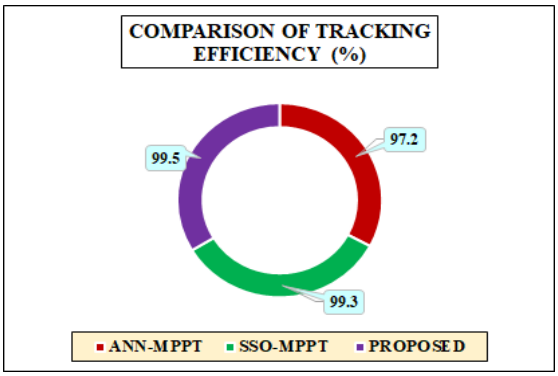

Figure 20 Analysis of tracking efficiency

Figure 20 displays an analysis of tracking efficiency for MPPT approaches like ANN [24], SSO [27] and developed MPPT approach. An ANN approach has the efficacy of 97.2% and SSO approach has the efficacy of 99.3% than developed approach that attains the maximum efficiency of 99.5%, establishing its superior ability in accurately and reliably tracking the highest power.

IV. CONCLUSION

This paper presents a Hybrid Renewable Energy System (HRES)–based EV charging station integrating both solar and wind energy sources. A High-Gain Interleaved Boost (HGIB) converter is employed to enhance the PV system voltage, providing improved voltage gain. The Maximum Power Point Tracking (MPPT) is achieved using a Flying Squirrel Optimized (FSO) Artificial Neural Network (ANN), delivering precise power extraction under varying environmental conditions. Additionally, a Doubly Fed Induction Generator–Wind Energy Conversion System (DFIG-WECS) supplies excess power to the system when needed. Energy exchange between the EV battery and the DC bus is managed by a bidirectional buck-boost converter, supporting efficient charging and discharging operations while enabling smart energy management and vehicle-to-grid functionality. MATLAB/Simulink simulations, compared with conventional approaches, demonstrate a converter efficiency of 95.23%. The proposed HRES design thus provides a sustainable and reliable solution for clean energy–based EV charging infrastructure.

Conflict of interest statement

Authors declare that they do not have any conflict of interest.

REFERENCES

[1] A. K. Karmaker, M. A. Hossain, H. R. Pota, A. Onen and J. Jung, "Energy Management System for Hybrid Renewable Energy-Based Electric Vehicle Charging Station," in IEEE Access, vol. 11, pp. 27793-27805, 2023.

[2] Kavin, K. S., and P. Subha Karuvelam. "PV-based grid interactive PMBLDC electric vehicle with high gain interleaved DC-DC SEPIC Converter." IETE Journal of Research 69, no. 7 (2023): 4791-4805.

[3] Priya, ATR Krishna, and R. Anuja. "High-Performance Deep Learning Classifier for Predicting Cyclones Based On Rain Optimization Algorithm."

[4] Vidhya, H; Abinaya, I; Karthik, M; Gandhi, RR Rubia; "FLC based Speed Control of Brushless DC Motor using C2000" "International Journal of Research in Engineering, Science, and Management", 2, 2019.

[5] Kavin, K. S., P. Subha Karuvelam, Abhinav Pathak, T. R. Premila, R. Hemalatha, and Tharwin Kumar. "Modelling and analysis of hybrid fuzzy tuned PI controller based PMBLDC motor for electric vehicle applications." SSRG International Journal of Electrical and Electronics Engineering 10, no. 2 (2023): 8-18.

[6] Karthik, M; Abinaya, I; Deepa, B; Devi, R Nithya; "A Review on Wind Turbines by PMSG Generator For Power Generation".

[7] Mohan, Harin M., and Santanu Kumar Dash. "Renewable energy-based DC microgrid with hybrid energy management system supporting electric vehicle charging system." Systems 11, no. 6 (2023): 273.

[8] Varanasi, Praveen Kumar, S. Nagaraja Rao, and Punithavathi Duraiswamy. "Intelligent Control of Double Boost Converter Interfaced with Multilevel Inverter for Electrical Vehicle Applications." Journal of The Institution of Engineers (India): Series B 106, no. 3 (2025): 939-947.

[9] Naresh, S. V. K., Sankar Peddapati, and Mamdouh L. Alghaythi. "Non-isolated high gain quadratic boost converter based on inductor's asymmetric input voltage." IEEE Access 9 (2021): 162108-162121.

[10] Zhao, Jiawei, and Daolian Chen. "Switched-capacitor high voltage gain Z-source converter with common ground and reduced passive component." IEEe Access 9 (2021): 21395-21407.

[11] Esmaeili, Soroush, Morteza Shekari, Milad Rasouli, Sara Hasanpour, Ashraf Ali Khan, and Hossein Hafezi. "High gain magnetically coupled single switch quadratic modified SEPIC DC-DC converter." IEEE Transactions on Industry Applications 59, no. 3 (2023): 3593-3604.

[12] Preethiraj, P. M., and J. Belwin Edward. "Design of novel DC-DC interleaved boost converter for BLDC application." Heliyon 10, no. 22 (2024).

[13] Hashemzadeh, Seyed Majid, Seyed Hossein Hosseini, Ebrahim Babaei, and Mehran Sabahi. "A soft switched high step-up DC-DC converter based on VMC and coupled inductor for photovoltaic energy applications." IET Renewable Power Generation 17, no. 6 (2023): 1583-1596.

[14] Hafeez, Muhammad Annas, Ahmer Naeem, Muhammad Akram, Muhammad Yaqoob Javed, Aamer Bilal Asghar, and Yong Wang. "A novel hybrid MPPT technique based on Harris hawk optimization (HHO) and perturb and observer (P&O) under partial and complex partial shading conditions." Energies 15, no. 15 (2022): 5550.

[15] Ibrahim, Mohammad Haziq, Swee Peng Ang, Muhammad Norfauzi Dani, Mohammad Ishlah Rahman, Rafidah Petra, and Sheik Mohammed Sulthan. "Optimizing step-size of perturb & observe and incremental conductance MPPT techniques using PSO for grid-tied PV system." IEEE access 11 (2023): 13079-13090.

[16] Sabir, Bushra, Shiue-Der Lu, Hwa-Dong Liu, Chang-Hua Lin, Adil Sarwar, and Liang-Yin Huang. "A novel isolated intelligent adjustable buck-boost converter with hill climbing MPPT algorithm for solar power systems." Processes 11, no. 4 (2023): 1010.

[17] Priya, ATR Krishna, and A. Yazhini. "Integrating Whale Optimization Algorithm and Machine Learning for Efficient Traffic Management."

[18] Xia, Kun, Yin Li, and Benjing Zhu. "Improved photovoltaic MPPT algorithm based on ant colony optimization and fuzzy logic under conditions of partial shading." IEEE Access 12 (2024): 44817-44825.

[19] Hilali, Abdelilah, Yahya Mardoude, Ali Essahlaoui, Abderrafii Rahali, and Najib El Ouanjli. "Migration to solar water pump system: Environmental and economic benefits and their optimization using genetic algorithm Based MPPT." Energy Reports 8 (2022): 10144-10153.

[20] Huang, Boyan, Kai Song, Shulin Jiang, Zhenqing Zhao, Zhiqiang Zhang, Cong Li, and Jiawen Sun. "A Robust Salp Swarm Algorithm for Photovoltaic Maximum Power Point Tracking Under Partial Shading Conditions." Mathematics 12, no. 24 (2024): 3971.

[21] Nagadurga, T., P. V. R. L. Narasimham, and V. S. Vakula. "Global maximum power point tracking of solar photovoltaic strings under partial shading conditions using cat swarm optimization technique." Sustainability 13, no. 19 (2021): 11106.

[22] Hadj Salah, Zahra Bel, Saber Krim, Mohamed Ali Hajjaji, Badr M. Alshammari, Khalid Alqunun, Ahmed Alzamil, and Tawfik Guesmi. "A new efficient cuckoo search MPPT algorithm based on a super-twisting sliding mode controller for partially shaded standalone photovoltaic system." Sustainability 15, no. 12 (2023): 9753.

[23] Kumar P K, V. ., J J, J., C, N. ., Manasa B, L. ., M, D. ., & D, M. . (2023). Design and Implementation of Modified Zeta Converter for Solar Water Pumping Application. International Journal on Recent and Innovation Trends in Computing and Communication, 11(8s), 01–09.

[24] K. S. Kavin, P. Subha Karuvelam, Naresh Kumar, Siddheswar Kar, Riyaz A. Rahiman, Sharda Patwa," Coupled inductor interleaved boost converter with ANN and RNN based MPPT algorithm for PV system", International Journal of Applied Power Engineering (IJAPE) Vol. 13, No. 3, September 2024, pp. 616~627.

[25] Ahmadi, L., Siadatan, A., Afjei, E. & Javadi, S. An efficient interleaved boost DC–DC converter with high-voltage gain based on switched capacitor. Electric. Eng. 107 (1), 249–261. (2025).

[26] Mansour, A. S., Amer, A. H. H., El-Kholy, E. E. & Zaky, M. S. High gain DC/DC converter with continuous input current for renewable energy applications. Sci. Reports. 12(1), 12138. (2022).

[27] A.F.Mirza,M.Mansoor,Q.Ling,B.Yin,andM.Y.Javed,''Asalp-swarm optimization based MPPT technique for harvesting maximum energy from PVsystems under partial shading conditions,'' Energy Convers. Manage., vol. 209, Apr. 2020, Art. no. 112625.